Commun. Comput. Phys.
doi: 10.4208/cicp.070710.100111a

Vol. **10**, No. 5, pp. 1257-1279
November 2011

A High Order Spectral Volume Formulation for Solving Equations Containing Higher Spatial Derivative Terms: Formulation and Analysis for Third Derivative Spatial Terms Using the LDG Discretization Procedure

Ravi Kannan*

CFD Research Corporation, 215 Wynn Drive, Huntsville, AL 35805, USA.

Received 7 July 2010; Accepted (in revised version) 10 January 2011

Available online 2 August 2011

Abstract. In this paper, we develop a formulation for solving equations containing higher spatial derivative terms in a spectral volume (SV) context; more specifically the emphasis is on handling equations containing third derivative terms. This formulation is based on the LDG (Local Discontinuous Galerkin) flux discretization method, originally employed for viscous equations containing second derivatives. A linear Fourier analysis was performed to study the dispersion and the dissipation properties of the new formulation. The Fourier analysis was utilized for two purposes: firstly to eliminate all the unstable SV partitions, secondly to obtain the optimal SV partition. Numerical experiments are performed to illustrate the capability of this formulation. Since this formulation is extremely local, it can be easily parallelized and a *h*-*p* adaptation is relatively straightforward to implement. In general, the numerical results are very promising and indicate that the approach has a great potential for higher dimension Korteweg-de Vries (KdV) type problems.

AMS subject classifications: 65

Key words: Spectral volume, LDG, higher spatial derivative terms, KDV, Fourier analysis.

1 Introduction

The spectral volume (SV) method was originally developed by Wang, Liu et al. and their collaborators for hyperbolic conservation laws on unstructured grids [20, 29–33]. The spectral volume method is a subset of the Godunov type finite volume method, which has been evolving for decades and has been a starting block for the development of a plethora of methods such as the *k*-exact finite volume [5, 8], MUSCL (Monotone

*Corresponding author. *Email address:* sunshekar@gmail.com (R. Kannan)

Upstream-centered Schemes for Conservation Laws) [27, 28], and the essentially non-oscillatory (ENO) [1, 11] methods. The spectral volume method can be viewed as an extension of the Godunov method to higher order by adding more degrees-of-freedom (DOFs) in the form of subcells in each cell (simplex). The simplex is referred to as a spectral volume (SV) and the subcells are referred to as control volumes (CV). Every simplex in the SV method consists of a "structured" arrangement of the above mentioned subcells (CVs). As in the finite volume method, the unknowns (or DOFs) are the subcell-averaged solutions. A finite volume procedure is employed to update the DOFs. The spectral volume method shares many similar properties with the discontinuous Galerkin (DG) [6, 7] and the spectral difference (SD) [18, 24] methods, such as discontinuous solution space, sharing multiple degrees of freedom within a single element and compactness. They mainly differ on how the DOFs are chosen and updated. Since the DG is a derivative of the finite element method, most implementations use the elemental nodal values as DOF, though some researchers use the equally valid modal approaches. Although both of the above approaches are mathematically identical, at least for linear equations, different choices of DOFs are used by various researchers result in different efficiency and numerical properties. The spectral volume being a derivative of the finite volume has subcell averages as its DOF while the spectral difference has point wise values as DOF. In terms of complexity, DG requires both volume and surface integrations. In contrast, SV requires only surface integrations and the SD requires differentiations.

The SV method was successfully implemented for 2D Euler [32] and 3D Maxwell equations [20]. The quadrature free formulation was implemented by Harris et al. [9]. A *h-p* adaptation was also carried out in 2D [10]. Recently Sun et al. [25] implemented the SV method for the Navier Stokes equations using the LDG [7] approach to discretize the viscous fluxes. Kannan and Wang [14, 17] conducted some Fourier analysis for a variety of viscous flux formulations. Kannan implemented the SV method for the Navier Stokes equations using the LDG2 (which is an improvised variant of the LDG approach) [15] and DDG approaches [16]. Even more recently, Kannan extended the SV method to solve the moment models in semiconductor device simulations [12, 13].

In this paper, we develop a formulation for solving equations containing third spatial derivative terms in a SV context. This formulation borrows ideas from Yan et al. [34, 35] for efficiently implementing the LDG method. A linear Fourier analysis is performed to test the accuracy of this formulation. The Fourier analysis was utilized for two purposes: firstly to eliminate all the unstable SV partitions, secondly to obtain the optimal SV partition. The maximum allowable non-dimensional time step was determined for these optimal partitions.

The paper is organized as follows. In the next section, we review the basics of the SV method. The LDG formulation for high order spatial derivatives is presented in Section 3. A detailed linear analysis is performed for the LDG formulation in Section 4. Section 5 presents with the different test cases conducted in this study. Finally conclusions from this study are summarized in Section 6.

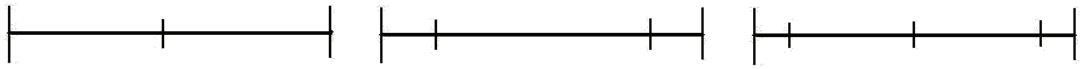

(a) (b) (c)

Figure 1: Partitions of a SV in 1D. (a): Linear reconstruction; (b): Quadratic reconstruction; (c): Cubic reconstruction.

2 Basics of the spectral volume method

2.1 Formulation in 1D

Consider the general conservation equation

$$\frac{\partial Q}{\partial t}+\frac{\partial\big(f_i(Q)-f_v(Q)\big)}{\partial x}=0, \tag{2.1}$$

in a one dimensional domain Ω with appropriate initial and boundary conditions. In (2.1), x refers to the Cartesian coordinate and $(x)\in\Omega$, $t\in[0,T]$ denotes time, Q is the vector of conserved variables, and f_i and f_v are the inviscid and viscous fluxes respectively. Domain Ω is discretized into I non overlapping sub cells. In the SV method, the simplex grid cells are called SVs, denoted S_i, which are further partitioned into CVs, denoted C_{ij}, which depend on the degree of the polynomial reconstruction. Fig. 1 shows linear, quadratic and cubic partitions in 1D. The partitions were originally determined for a linear advection equation using a linear Fourier analysis [26]. One of the outcomes of this paper is to obtain stable and accurate partitions for equations having third derivatives.

We need N unknown control volume solution averages (or DOFs) to construct a degree k polynomial. N is calculated using the below formula (in 1D)

$$N=k+1, \tag{2.2}$$

where k is the degrees of the polynomial, constructed using the CV solution averages. The CV averaged conserved variable for C_{ij} is defined as

$$\overline{Q}_{i,j}=\frac{1}{V_{i,j}}\int_{C_{i,j}}QdV,\quad j=1,\cdots,N,\ i=1,\cdots,I, \tag{2.3}$$

where $V_{i,j}$ is the volume of C_{ij}. Given the CV averaged conserved variables, a degree k polynomial can be constructed such that it is $(k+1)^{\text{th}}$ order approximation to Q. In other words, we can write the polynomial as

$$p_i(x)=\sum_{j=1}^{N}L_j(x)\overline{Q}_{i,j}, \tag{2.4}$$

where the shape functions $L_j(x,y)$ satisfy

$$\frac{1}{V_{i,j}}\int_{C_{i,j}}L_n(x)dV=\delta_{j,n}. \tag{2.5}$$

Eq. (2.1) is integrated over the C_{ij}. This results in the following equation

$$\frac{\partial \overline{Q}}{\partial t}+\frac{1}{V_{i,j}}\sum_{r=1}^{K}\int_{Ar}(\vec{F}\cdot\vec{n})dA=0, \tag{2.6}$$

where $\overline{F}=(f_i-f_v)$, Ar represents the r^{th} face of C_{ij}, $\vec{n}$ is the outward unit normal vector of Ar and K is the number of faces in C_{ij} (two in 1D). The fluxes are discontinuous across the SV interfaces. The inviscid fluxes can be handled using a numerical Riemann flux, such as upwinding, the Rusanov flux [22], the Roe flux [21] or AUSM flux [19]. In this manuscript, upwinding is employed to handle the inviscid fluxes. The handling of the viscous fluxes is discussed below.

2.2 Spectral volume formulation for the diffusion equation

The following diffusion equation is considered first in domain Ω with appropriate initial and boundary conditions

$$\frac{\partial u}{\partial t}-\nabla\cdot(\mu\nabla u)=0, \tag{2.7}$$

where μ is a positive diffusion coefficient. We define an auxiliary variable

$$\vec{q}=\nabla u. \tag{2.8}$$

Eq. (2.7) then becomes

$$\frac{\partial u}{\partial t}-\nabla\cdot(\mu\vec{q})=0. \tag{2.9}$$

Using the Gauss-divergence theorem, we obtain

$$\overline{\vec{q}}_{ij}V_{ij}=\sum_{r=1}^{K}\int_{Ar}u\cdot\vec{n}dA, \tag{2.10a}$$

$$\frac{d\overline{u}_{ij}}{dt}V_{ij}-\sum_{r=1}^{K}\int_{Ar}\mu\vec{q}\cdot\vec{n}dA=0, \tag{2.10b}$$

where $\overline{\vec{q}}_{ij}$ and $\overline{u}_{ij}$ are the CV averaged gradient and solution in C_{ij}. As the solution u is cell-wise continuous, u and $\vec{q}$ at SV boundaries are replaced by numerical fluxes $\underline{\vec{q}}$ and $\underline{u}$. The above equations thus become

$$\overline{\vec{q}}_{ij}V_{ij}=\sum_{r=1}^{K}\int_{Ar}\underline{u}\cdot\vec{n}dA, \tag{2.11a}$$

$$\frac{d\overline{u}_{ij}}{dt}V_{ij}-\sum_{r=1}^{K}\int_{Ar}\mu\underline{\vec{q}}\cdot\vec{n}dA=0. \tag{2.11b}$$

The commonly used approach for obtaining the numerical fluxes is the LDG approach. In this approach, the numerical fluxes are defined by alternating the direction in the following manner [25]

$$\underline{u} = u_L, \tag{2.12a}$$

$$\underline{\vec{q}} = \vec{q}_R, \tag{2.12b}$$

where u_R and u_L are the left and right state solutions of the CV face in consideration and $\vec{q}_L$ and $\vec{q}_R$ are the left and right state solution gradients of the face (of the CV) in consideration. Thus if the CV face lies on the SV boundary, $u_L \neq u_R$ and $\vec{q}_L \neq \vec{q}_R$ (assuming that the function is not smooth).

3 SV for higher spatial derivatives

We will explain the procedure using a linear equation; consider the following simple linear equation with the appropriate initial and boundary conditions

$$u_t + u_{xxx} = 0. \tag{3.1}$$

Rewriting the above into a first order system yields:

$$u_t + p_x = 0, \qquad p = q_x, \qquad q = u_x. \tag{3.2}$$

Integrating Eq. (3.2) over the CV and application of Gauss-divergence theorem yields:

$$\frac{d\overline{u}_{ij}}{dt} V_{ij} + \sum_{r=1}^{K} \int_{Ar} \vec{p} \cdot \vec{n} dA = 0, \tag{3.3a}$$

$$\overline{\vec{p}}_{ij} V_{ij} = \sum_{r=1}^{K} \int_{Ar} q \cdot \vec{n} dA, \tag{3.3b}$$

$$\overline{\vec{q}}_{ij} V_{ij} = \sum_{r=1}^{K} \int_{Ar} u \cdot \vec{n} dA. \tag{3.3c}$$

u, p and q at SV boundaries are replaced by numerical fluxes $\underline{u}$, $\underline{\vec{p}}$ and $\underline{\vec{q}}$. Eqs. (3.3a), (3.3b) and (3.3c) can be solved by extending the LDG method discussed in [14, 15, 25] to higher derivatives (shown in the below subsection).

3.1 The LDG formulation

In this approach, the numerical fluxes are defined by alternating the direction of the numerical fluxes. There are two choices:

- Choice a: $\underline{u} = u_L, \quad \underline{\vec{q}} = \vec{q}_R, \quad \underline{\vec{p}} = \vec{p}_R;$ (3.4)
- Choice b: $\underline{u} = u_R, \quad \underline{\vec{q}} = \vec{q}_R, \quad \underline{\vec{p}} = \vec{p}_L.$ (3.5)

Though there are a total of eight choices (two for each variable), six of them are unconditionally unstable. More details can be found in [34, 35]. The size of the stencil is 5 (optimal).

4 Fourier analysis for the new formulation

In this analysis, we follow a technique described by Zhang and Shu [36] and focus on linear, quadratic and cubic reconstructions. The SV is partitioned into two equal CVs for the second order simulations. The CVs for the third and the fourth order are clustered toward the SV boundaries. The locations of the CV faces (i.e., nodes in 1D) were based on the Gauss quadrature points. For the sake of simplicity, let us first consider a linear partition shown in Fig. 2. In this case, all the formulations can be cast in the following form:

$$\frac{d}{dt}\begin{bmatrix}\overline{u}_{j,1}\\ \overline{u}_{j,2}\end{bmatrix}=A\begin{bmatrix}\overline{u}_{j-2,1}\\ \overline{u}_{j-2,2}\end{bmatrix}+B\begin{bmatrix}\overline{u}_{j-1,1}\\ \overline{u}_{j-1,2}\end{bmatrix}+C\begin{bmatrix}\overline{u}_{j,1}\\ \overline{u}_{j,2}\end{bmatrix}+D\begin{bmatrix}\overline{u}_{j+1,1}\\ \overline{u}_{j+1,2}\end{bmatrix}+E\begin{bmatrix}\overline{u}_{j+2,1}\\ \overline{u}_{j+2,2}\end{bmatrix}, \quad (4.1)$$

where A, B, C, D and E are constant matrices. We now seek a general solution of the following form

$$u(x,t)=\hat{u}_k(t)e^{ikx}, \quad (4.2)$$

where k is the index of modes ($k=1,2,\cdots,$) representing the wave number and $\hat{u}_k$ is the amplitude of the given wave. Obviously, the analytical solution for Eq. (3.1) is $u(x,t)=e^{i(kx+k^3t)}$. The solution we are looking for can be expressed as

$$\begin{bmatrix}\overline{u}_{j,1}\\ \overline{u}_{j,2}\end{bmatrix}=\begin{bmatrix}\hat{u}_{k,1}\\ \hat{u}_{k,2}\end{bmatrix}e^{ikx_{j,\frac{3}{2}}}. \quad (4.3)$$

Substituting Eq. (4.3) into Eq. (4.1), we obtain the advancement equation:

$$\begin{bmatrix}\hat{u}'_{k,1}\\ \hat{u}'_{k,2}\end{bmatrix}=G(k,h)\begin{bmatrix}\hat{u}_{k,1}\\ \hat{u}_{k,2}\end{bmatrix}, \quad (4.4)$$

where the amplification matrix is given by

$$G=e^{-2ikh}A+e^{-ikh}B+C+e^{ikh}D+e^{2ikh}E. \quad (4.5)$$

The above method can be easily extended to 3rd and 4th orders. In general, all but one of the eigen values of G is made up of spurious modes and is damped rapidly. This is under the assumption that the scheme is stable (ensured by making sure that the real part of the eigen values is non positive). The error associated with the scheme and the convergence properties can be determined by analyzing the non spurious mode. It must be noted that both discretization methods (Eq. (3.4) or Eq. (3.5)) will yield identical results during this analysis procedure.

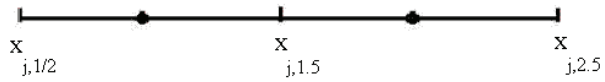

Figure 2: Linear spectral volume in 1D.

4.1 Second order spatial analysis

Fig. 3 shows the variation of the real component of the principal eigen value with respect to the non dimensional frequency $\xi = kh$ for the second order SV. As expected all the values in Fig. 3 are non-positive. Similarly Fig. 4 shows the deviation between the imaginary components of the principal (numerical) eigen value and the analytical eigen value (i.e., $i\xi^3$) as a function of ξ.

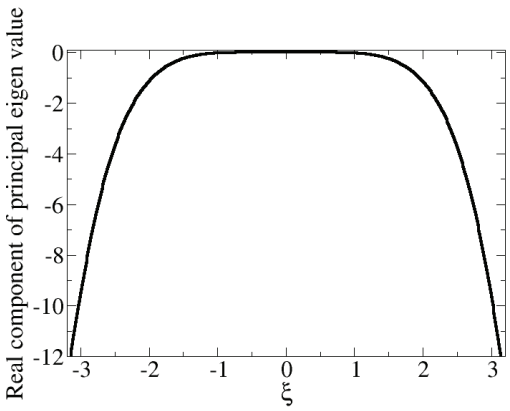

Figure 3: Plot of the real component of the principal eigen value as a function of the non-dimensional frequency for the second order SV.

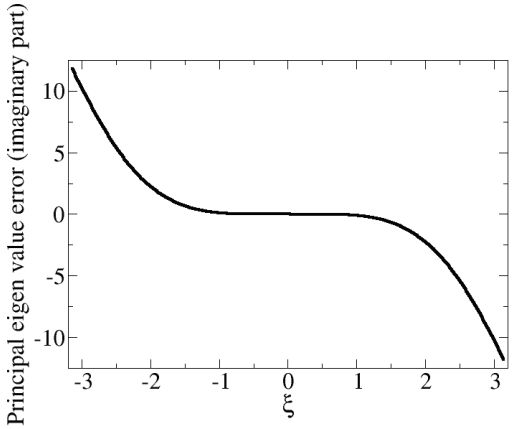

Figure 4: Plot of the error associated with the imaginary component of the principal eigen value as a function of the non-dimensional frequency for the second order SV.

4.2 Third order spatial analysis

The third order SV of unit length has its interior CV boundaries given by the following local coordinates: $\{0,d,1-d,1\}$, where d is the length of the first CV in the SV. The stability and the accuracy of the formulation proposed in this manuscript depend on the value of d. Fig. 5 shows the L_1 and L_∞ dissipation and dispersion errors as a function of d. 315 points were chosen to represent the interval between 0 and π. Numerical experiments were also conducted with 629 points and the results were almost identical w.r.t the errors as well as stability. This proves that the grid independence is attained.

The dissipation error (for a non dimensional frequency $\xi = kh$) is the real component of the principal (numerical) eigen value. The dispersion error (for a non dimensional frequency $\xi = kh$) is the deviation between the imaginary components of the principal (numerical) eigen value and the analytical eigen value (i.e., $i\xi^3$). The maximum of the real

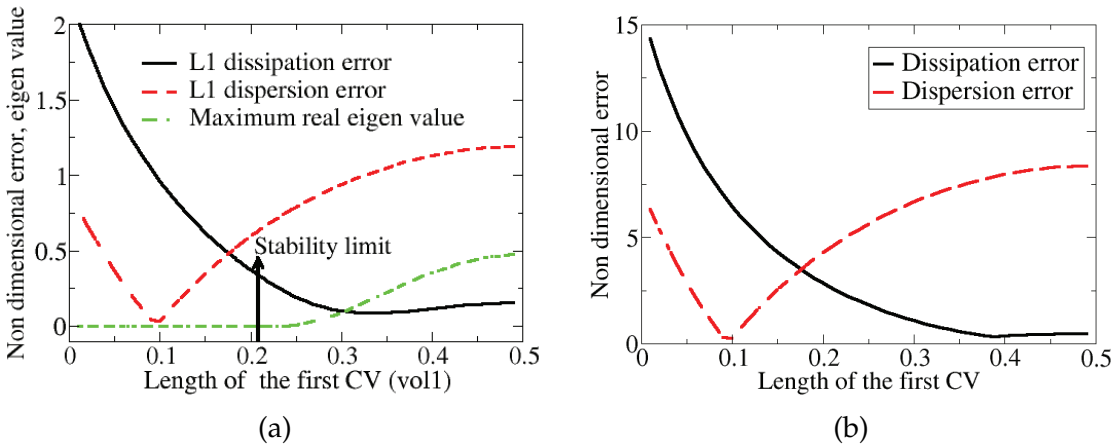

Figure 5: Stability and accuracy properties for the third order SV. (a): L_1 error; (b): L_∞ error.

component of the eigen values is also plotted as a function of d in the above mentioned figure. This value is positive beyond a critical d ($d_{\text{critical}} = 0.204$). This implies that the amplitude of the waves will grow exponentially in time for a SV partition, wherein $d > d_{\text{critical}}$. This is regardless of the fact that the SV partitions with $d > d_{\text{critical}}$ have smaller L_1 dissipation errors than the SV partitions with $d < d_{\text{critical}}$.

The SV partition, having $d = 0.1$ has the lowest L_1 dispersion error and a reasonable L_1 and L_∞ dissipation errors; this will be used in the remainder of the paper.

Fig. 6 shows the variation of the real component of the principal eigen value with respect to the non dimensional frequency $\xi = kh$ for the third order SV where $d = 0.1$. As expected all the values in Fig. 6 are non-positive. Similarly Fig. 7 shows the deviation between the imaginary components of the principal (numerical) eigen value and the an-

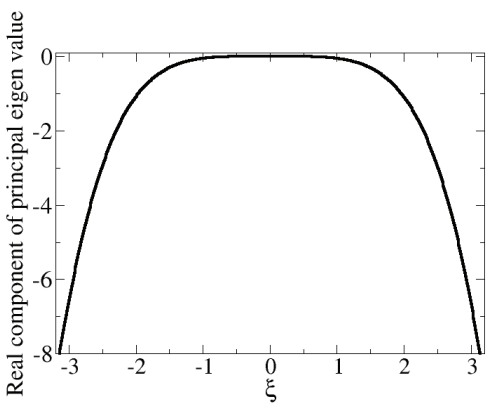

Figure 6: Plot of the real component of the principal eigen value as a function of the non-dimensional frequency for the third order SV with $d = 0.1$.

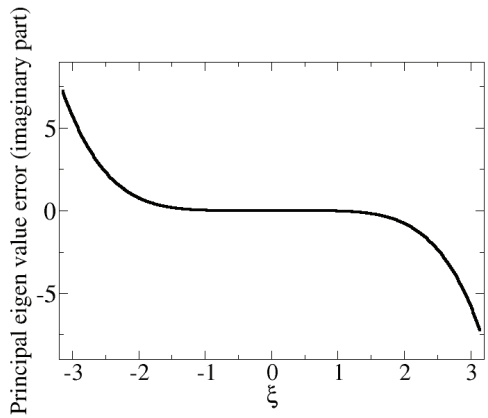

Figure 7: Plot of the error associated with the imaginary component of the principal eigen value as a function of the non-dimensional frequency for the third order SV with $d = 0.1$.

alytical eigen value (i.e., $i\xi^3$) as a function of ξ. Unsurprisingly, the principal eigen value of the third order scheme shows more fidelity than its second order counterparts.

4.3 Fourth order spatial analysis

The fourth order SV of unit length has its interior CV boundaries given by the following local coordinates: $\{0,d,0.5,1-d,1\}$, where d is the length of the first CV in the SV. As mentioned earlier, the stability and the accuracy of the formulation proposed in this manuscript depend on the value of d. Fig. 8 shows the L_1 dissipation and dispersion errors as a function of d. The maximum of the real component of the eigen values is also plotted as a function of d in the above mentioned figure. This value is positive beyond a critical d ($d_{\text{critical}} = 0.112$).

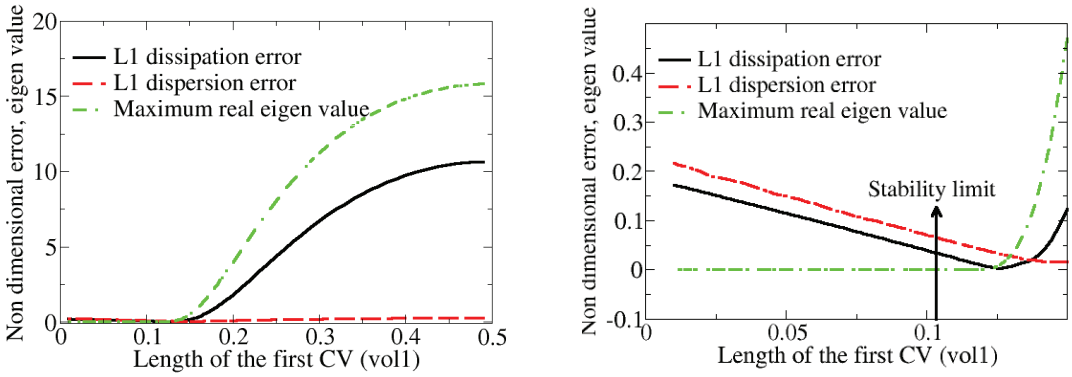

(a) (b)

Figure 8: Stability and accuracy properties for the fourth order SV. (a): Properties across the entire range; (b): Properties at small values of the first CV.

It can be seen (from Fig. 8) that the SV partition, having $d = d_{\text{critical}}$ has the lowest L_1 dispersion error and dissipation errors among the stable partitions. However many equations used in the modeling of real life physics, contain both first derivative and higher spatial derivative terms. It has been shown by Van Den Abeele et al. [26] that a SV partition, having $d = 0.1$ results in very low dispersion error and dissipation errors for a linear advecting wave. Since the errors (dispersion and dissipation) at $d = 0.1$ and $d = d_{\text{critical}}$ are nearly identical, it would be reasonable to use a SV partition with $d = 0.1$ for a general problem; this will be used in the remainder of the paper.

Fig. 9 shows the variation of the real component of the principal eigen value with respect to the non dimensional frequency ξ for the third order SV where d=0.1. As expected all the values in Fig. 9 are non-positive. Similarly Fig. 10 shows the deviation between the imaginary components of the principal (numerical) eigen value and the analytical eigen value (i.e., $i\xi^3$) as a function of ξ. Once again, the principal eigen value of the fourth order scheme shows more fidelity than its second and third order counterparts.

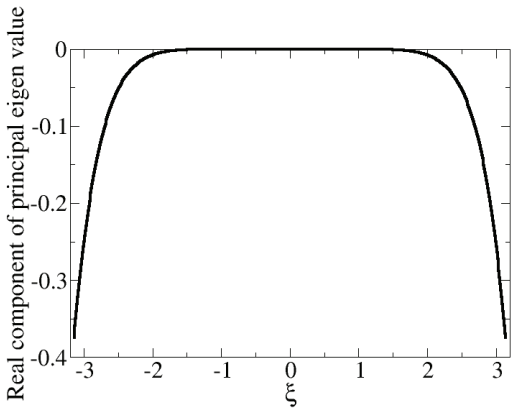

Figure 9: Plot of the real component of the principal eigen value as a function of the non-dimensional frequency for the fourth order SV with $d=0.1$.

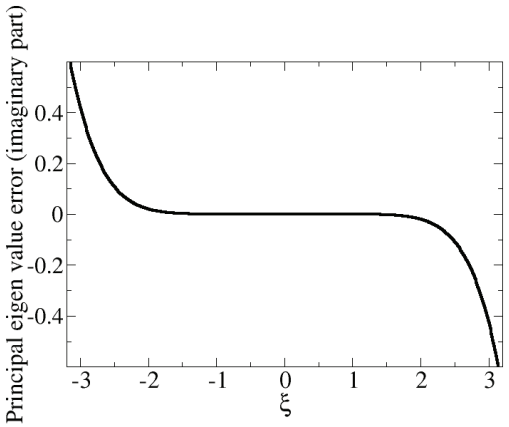

Figure 10: Plot of the error associated with the imaginary component of the principal eigen value as a function of the non-dimensional frequency for the fourth order SV with $d=0.1$.

4.4 Second order temporal analysis

In this section, we compute the time step requirements of a third order temporal scheme in conjunction to the current SV formulation. We employ the standard Taylor expansion to link $\lfloor \hat{u}_k^{'n} \rfloor$ (the CV averaged solution vector at the current time step) to $\lfloor \hat{u}_k^{'n+1} \rfloor$ (the CV averaged solution vector at the next time step):

$$\lfloor \hat{u}_k^{'n+1} \rfloor = \lfloor \hat{u}_k^{'n} \rfloor + \Delta t \frac{\partial [\hat{u}_k^{'n}]}{\partial t} + \frac{\Delta t^2}{2} \frac{\partial^2 [\hat{u}_k^{'n}]}{\partial t^2} + \frac{\Delta t^3}{6} \frac{\partial^3 [\hat{u}_k^{'n}]}{\partial t^3}. \tag{4.6}$$

Combining Eqs. (4.4) and (4.6), we obtain the following advancement equation:

$$\lfloor \hat{u}_k^{'n+1} \rfloor = [H] \lfloor \hat{u}_k^{'n} \rfloor, \tag{4.7}$$

where $[H]$ is

$$[H] = [I] + [G]\Delta t + \frac{[G]^2}{2}\Delta t^2 + \frac{[G]^3}{6}\Delta t^3, \tag{4.8}$$

with $[I]$ being the Identity matrix. The eigen values of $[H]$ matrix were computed. The moduli of each of the above computed eigen values need to be less than unity to ensure a stable system.

A maximum non-dimensional time step ($\tau = \mu \Delta t / \Delta x^3$) of 0.1109 was required for obtaining a stable solution. This is the non-dimensional time step, at which the maximum modulus of the eigen values of $[H]$ starts exceeding unity.

Table 1: Maximum non-dimensional time step ($\tau = \mu\Delta t/\Delta x^3$) for obtaining stable solutions for the third order formulation. The regions of locally stability are also listed.

d	maximum non-dimensional time step	Regions of local stability
0.20	0.08088	–
0.19	0.08065	–
0.18	0.08037	–
0.17	0.08003	–
0.16	0.07963	–
0.15	0.07917	–
0.14	0.07864	–
0.13	0.07804	–
0.12	0.07737	–
0.11	0.07662	–
0.10	0.07578	–
0.09	0.07485	–
0.08	0.07383	–
0.07	0.07271	–
0.06	0.06101	0.06103-0.06110 0.06112-0.06133 0.06135-0.06147
0.05	0.03377	0.03379-0.03488 0.03490-0.03493 0.03495-0.03509

4.5 Third order temporal analysis

Table 1 lists the maximum non-dimensional time step ($\tau = \mu\Delta t/\Delta x^3$) required for obtaining a stable solution. The variation of the maximum non-dimensional time step as a function of d is also shown in Fig. 11. However, stability analysis shows that the formulation is stable for a small range of non-dimensional time steps, which are higher than the computed stability cut-offs. This is due to the non-linear nature of Eq. (4.8). Some of these pockets are given in Table 1.

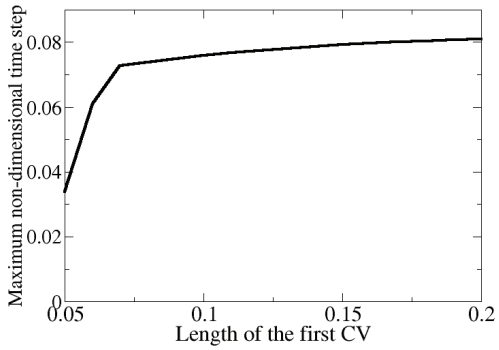

Figure 11: Maximum non-dimensional time step ($\tau = \mu\Delta t/\Delta x^3$) for obtaining stable solutions for the third order formulation.

Table 2: Maximum non-dimensional time step ($\tau=\mu\Delta t/\Delta x^3$) for obtaining stable solutions for the fourth order formulation. The regions of locally stability are also listed.

d	maximum non-dimensional time step	Regions of local stability
0.11	0.05860	–
0.10	0.05961	–
0.09	0.06057	–
0.08	0.05723	0.05725-0.05790 0.05792-0.05856 0.05890-0.05920
0.07	0.04537	0.04656-0.04668 0.04727-0.04733 0.04745-0.04775
0.06	0.03495	0.03497-0.03740 0.03742-0.03748 0.03750-0.03756
0.05	0.02692	0.02694-0.02707 0.02727-0.02738 0.02783-0.02792
0.04	0.01521	0.01523-0.01538 0.01680-0.01726 0.01744-0.01751
0.03	0.00971	0.00972-0.01001 0.01004-0.01009 0.01011-0.01022

4.6 Fourth order temporal analysis

Table 2 lists the maximum non-dimensional time step ($\tau=\mu\Delta t/\Delta x^3$) required for obtaining a stable solution. This variation of the maximum non-dimensional time step as a function of d is also shown in Fig. 12. The locally occurring stable regions are also given in Table 2. It can be seen that the fourth order scheme has more locally stable regions than the third order scheme. This is due to the fact that the eigen value computation procedure is more non-linear for the fourth order scheme.

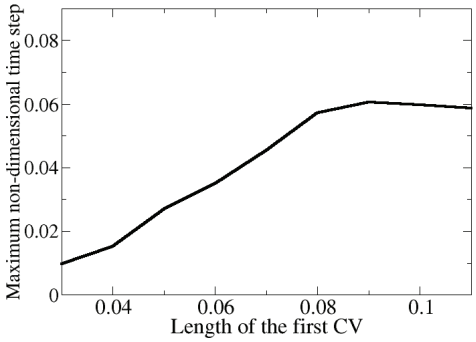

Figure 12: Maximum non-dimensional time step ($\tau=\mu\Delta t/\Delta x^3$) for obtaining stable solutions for the fourth order formulation.

4.7 Numerical verification of stable and unstable partitions

Numerical simulations were performed in order to test the above stability related results. We compute the solution of the below equation:

$$u_x + u_{xxx} = 0, \tag{4.9}$$

with an initial condition $u(x,0)=\exp(x)$ over the interval $[0,2\pi]$. The following boundary conditions were applied:

$$u(0,t)=\exp(-t), \qquad u_x(2\pi,t)=\exp(2\pi-t), \qquad u_{xx}(2\pi,t)=\exp(2\pi-t), \tag{4.10}$$

with the analytical solution to Eq. (4.9) being: $u(x,t)=\exp(x-t)$.

Table 3 shows the L_2 and L_∞ errors for various combinations of d for a third order simulation. A non dimensional time step of 0.01 was employed for the current simulation. This time stepping is slightly smaller than the ones mentioned in Table 1, so as to take care of non linear and non-periodic effects. The following can be observed: (1) The $d=0.211$ case diverges extremely fast, (2) The case corresponding to $d=0.1$ generates smaller errors than the one corresponding to $d=0.15$. These results are in accord with the results of the stability analysis.

Table 4 shows the L_2 and L_∞ errors for various combinations of d for a fourth order simulation. A non dimensional time step of 0.005 was employed for the current simulation. The $d=0.146$ case diverges very fast, thus providing credence to the stability analysis. The $d=0.1$ case generates smaller errors than the $d=0.05$ case.

The actual accuracy analysis will be performed in Section 5.

Table 3: $u_t+u_{xxx}=0$, $u(x,0)=\exp(x)$. Boundary conditions given in Eq. (4.10). L_2 and L_∞ errors using uniform meshes for the third order simulations.

N	d	N-steps	L_2-error	L_∞-error
100	$\left(1-\frac{1}{\sqrt{3}}\right)*0.5\approx 0.211$	1	0.000152	0.00384
		2	0.000565	0.0279
		3	0.00475	0.367
		4	0.0717	4.97
		5	1.09	67.2
10	$\left(1-\frac{1}{\sqrt{3}}\right)*0.5\approx 0.211$	1	0.248	3.37
		2	3.40	29.8
		3	52.5	372
10	0.15	1e5	0.0369	0.0497
		2e5	0.0196	0.0264
100		1e5	0.000155	0.00160
		2e5	0.000151	0.00152
10	0.10	1e5	0.0182	0.0245
		2e5	0.00968	0.0130
100		1e5	0.000137	0.00156
		2e5	0.000134	0.00150

Table 4: $u_t+u_{xxx}=0$, $u(x,0)=\exp(x)$. Boundary conditions given in Eq. (4.10). L_2 and L_∞ errors using uniform meshes for the fourth order simulations.

N	d	N-steps	L_2-error	L_∞-error
100	$\frac{\sqrt{2}-1}{2\sqrt{2}}\approx 0.146$	1	3.28e-05	0.000443
		2	0.00309	0.0404
		3	0.294	3.83
		4	27.9	355
		5	2.66e03	3.37e04
10	$\frac{\sqrt{2}-1}{2\sqrt{2}}\approx 0.146$	1	0.279	2.24
		2	26.4	191
		3	2520	1.73e04
10	0.10	1e5	1.67e-03	2.26e-03
		2e5	1.22e-03	1.64e-03
100		1e5	4.97e-06	6.63e-05
		2e5	4.91e-06	6.54e-05
10	0.05	1e5	1.71e-03	2.96e-03
		2e5	1.57e-03	2.12e-03
100		1e5	5.01e-06	6.67e-05
		2e5	4.96e-06	6.62e-05

5 Test results

In this section, we provide numerical examples to illustrate the capability of the LDG based SV formulation for solving equations containing third spatial derivative terms. A three stage SSP Runge-Kutta scheme was used for time advancement [23]:

$$\overline{u}_i^{(1)}=\overline{u}_i^n-\Delta t R_i(\overline{u}^n), \tag{5.1a}$$

$$\overline{u}_i^{(2)}=\frac{3}{4}\overline{u}_i^n+\frac{1}{4}\left[\overline{u}_i^{(1)}-\Delta t R_i(\overline{u}^{(1)})\right], \tag{5.1b}$$

$$\overline{u}_i^{n+1}=\frac{1}{3}\overline{u}_i^n+\frac{2}{3}\left[\overline{u}_i^{(2)}-\Delta t R_i(\overline{u}^{(2)})\right]. \tag{5.1c}$$

5.1 Test case 1

We compute the solution of the linear equation:

$$u_t+u_{xxx}=0, \tag{5.2}$$

with an initial condition $u(x,0)=\sin x$ and periodic boundary conditions (periodicity $=2\pi$) over the interval $[0,2\pi]$. This equation has an analytical solution: $u(x,t)=\sin(x+t)$. Both uniform and non-uniform meshes were used in this study. Two types of non-uniform meshes were used. The first type had a recurring pattern of SVs of lengths 0.9Δ and 1.1Δ, where Δ was the length of the corresponding uniform SV. The second type had a recurring pattern of SVs of lengths 0.7Δ and 1.3Δ. An even number of SVs were

Table 5: $u_t+u_{xxx}=0$, $u(x,0)=\sin x$. Periodic boundary conditions over interval $[0,2\pi]$. L_2 and L_∞ errors using uniform meshes at $t=1$.

k	Grid	L_2-error	L_2-order	L_∞-error	L_∞-order
1	10	1.41e-2	–	4.78e-2	–
	20	3.55e-3	1.99	1.27e-2	1.91
	40	8.87e-4	2.00	3.22e-3	1.98
	80	2.22e-4	2.00	8.06e-4	2.00
2	10	7.31e-4	–	3.31e-3	–
	20	9.26e-5	2.98	4.19e-4	2.98
	40	1.16e-5	2.99	5.31e-5	2.98
	80	1.46e-6	3.00	6.69e-6	2.99
3	10	2.11e-5	–	1.21e-4	–
	20	1.32e-6	3.99	7.61e-6	3.99
	40	8.30e-8	4.00	4.79e-7	3.99
	80	5.19e-9	4.00	2.99e-8	4.00

Table 6: $u_t+u_{xxx}=0$, $u(x,0)=\sin x$. Periodic boundary conditions over interval $[0,2\pi]$. L_2 and L_∞ errors using non-uniform (repeating pattern of 0.9Δ and $1.1\Delta x$) meshes at $t=1$.

k	Grid	L_2-error	L_2-order	L_∞-error	L_∞-order
1	10	1.60e-2	–	5.83e-2	–
	20	4.08e-3	1.97	1.56e-2	1.90
	40	1.03e-3	1.99	3.96e-3	1.98
	80	2.57e-4	2.00	9.97e-4	1.99
2	10	8.81e-4	–	4.47e-3	–
	20	1.12e-4	2.97	5.74e-4	2.96
	40	1.41e-5	2.99	7.28e-5	2.98
	80	1.77e-6	3.00	9.16e-6	2.99
3	10	5.11e-5	–	2.41e-4	–
	20	3.26e-6	3.97	1.55e-5	3.96
	40	2.06e-7	3.98	9.81e-7	3.98
	80	1.30e-8	3.99	6.22e-8	3.98

used for all the test cases. The L_2 and L_∞ errors and orders of accuracies of the numerical solution at $t=1$ second are given in Tables 5-7. It can be seen that the formulation with k^{th} degree polynomial asymptotically attains a $(k+1)^{\text{th}}$ order of accuracy. This phenomenon is observed for both the uniform and the non-uniform meshes.

5.2 Test case 2

We compute the solution of the non-linear KdV equation [34,35]:

$$u_t-3(u^2)_x+u_{xxx}=0, \tag{5.3}$$

with an initial condition $u(x,0)=-2\text{sech}^2(x)$ over the interval $[-10,12]$. The following boundary conditions were applied:

$$u(-10,t)=g_1(t), \qquad u_x(12,t)=g_2(t), \qquad u_{xx}(12,t)=g_3(t), \tag{5.4}$$

Table 7: $u_t+u_{xxx}=0$, $u(x,0)=\sin x$. Periodic boundary conditions over interval $[0,2\pi]$. L_2 and L_∞ errors using non-uniform (repeating pattern of $0.7\Delta x$ and $1.3\Delta x$) meshes at $t=1$.

k	Grid	L_2-error	L_2-order	L_∞-error	L_∞-order
1	10	2.27e-2	–	7.44e-2	–
	20	5.87e-3	1.95	2.00e-2	1.89
	40	1.49e-3	1.98	5.12e-3	1.97
	80	3.75e-4	1.99	1.29e-3	1.99
2	10	1.27e-3	–	8.51e-3	–
	20	1.69e-4	2.91	1.16e-3	2.88
	40	2.20e-5	2.94	1.53e-4	2.91
	80	2.79e-6	2.98	1.97e-5	2.96
3	10	3.98e-4	–	1.31e-3	–
	20	2.62e-5	3.92	8.77e-5	3.90
	40	1.70e-6	3.95	5.71e-6	3.94
	80	1.08e-7	3.98	3.64e-7	3.97

where $g_i(t)$ is obtained from the analytical solution to Eq. (5.3): $u(x,t)=-2\text{sech}^2(x-4t)$.

The L_2 and L_∞ errors and orders of accuracies of the numerical solution at $t=0.5$ second are given in Tables 8-10. It can be seen that a full $(k+1)^{\text{th}}$ order of accuracy is asymptotically attained for the formulation with k^{th} degree polynomial, in spite of the problem being heavily non-linear. Once again, this phenomenon is observed for both the uniform and the non-uniform meshes.

Table 8: $u_t-3(u^2)_x+u_{xxx}=0$, $u(x,0)=-2\text{sech}^2(x)$. Domain over the interval $[-10,12]$. Boundary conditions given in Eq. (5.4). L_2 and L_∞ errors using uniform meshes at $t=0.5$.

k	Grid	L_2-error	L_2-order	L_∞-error	L_∞-order
1	10	2.29e-1	–	1.37e-0	–
	20	7.25e-2	1.66	5.45e-1	1.33
	40	2.08e-2	1.80	1.92e-1	1.50
	80	5.50e-3	1.92	6.05e-2	1.67
	160	1.40e-3	1.97	1.73e-2	1.80
	320	3.51e-4	2.00	4.51e-3	1.94
2	10	8.39e-2	–	7.70e-1	–
	20	1.23e-2	2.77	1.17e-1	2.71
	40	1.83e-3	2.75	2.01e-2	2.55
	80	2.46e-4	2.89	3.29e-3	2.61
	160	3.19e-5	2.95	4.69e-4	2.81
	320	3.99e-6	3.00	5.95e-5	2.98
3	10	2.80e-2	–	2.91e-1	–
	20	2.99e-3	3.23	3.37e-2	3.11
	40	2.81e-4	3.41	3.22e-3	3.39
	80	2.00e-5	3.81	2.94e-4	3.45
	160	1.31e-6	3.93	2.14e-5	3.78
	320	8.27e-8	3.99	1.38e-6	3.96

Table 9: $u_t-3(u^2)_x+u_{xxx}=0$, $u(x,0)=-2\text{sech}^2(x)$. Domain over the interval $[-10,12]$. Boundary conditions given in Eq. (5.4). L_2 and L_∞ errors using non-uniform (repeating pattern of $0.9\Delta x$ and $1.1\Delta x$) meshes at $t=0.5$.

k	Grid	L_2-error	L_2-order	L_∞-error	L_∞-order
1	10	2.62e-1	–	1.46e-0	–
	20	8.53e-2	1.62	6.01e-1	1.28
	40	2.50e-2	1.77	2.20e-1	1.45
	80	6.71e-3	1.90	7.11e-2	1.63
	160	1.72e-3	1.96	2.08e-2	1.77
	320	4.31e-4	2.00	5.47e-3	1.93
2	10	1.09e-1	–	1.06e0	–
	20	1.66e-2	2.71	1.65e-1	2.68
	40	2.51e-3	2.73	2.81e-2	2.56
	80	3.43e-4	2.87	4.57e-3	2.62
	160	4.41e-5	2.96	6.51e-4	2.81
	320	5.51e-6	3.00	8.31e-5	2.97
3	10	4.99e-2	–	4.09e-1	–
	20	5.18e-3	3.27	4.83e-2	3.08
	40	4.77e-4	3.44	4.81e-3	3.33
	80	3.45e-5	3.79	4.34e-4	3.47
	160	2.25e-6	3.94	3.20e-5	3.76
	320	1.42e-7	3.98	2.04e-6	3.97

Table 10: $u_t-3(u^2)_x+u_{xxx}=0$, $u(x,0)=-2\text{sech}^2(x)$. Domain over the interval $[-10,12]$. Boundary conditions given in Eq. (5.4). L_2 and L_∞ errors using non-uniform (repeating pattern of $0.7\Delta x$ and $1.3\Delta x$) meshes at $t=0.5$.

k	Grid	L_2-error	L_2-order	L_∞-error	L_∞-order
1	10	3.21e-1	–	1.82e-0	–
	20	1.14e-1	1.50	7.85e-1	1.21
	40	3.45e-2	1.72	2.97e-1	1.40
	80	9.38e-3	1.88	9.81e-2	1.60
	160	2.43e-3	1.95	2.91e-2	1.75
	320	6.11e-4	1.99	7.71e-3	1.92
2	10	2.45e-1	–	2.61e0	–
	20	3.80e-2	2.69	4.46e-1	2.55
	40	5.70e-3	2.74	7.21e-2	2.63
	80	8.18e-4	2.80	1.18e-2	2.61
	160	1.09e-4	2.90	1.72e-3	2.78
	320	1.39e-5	2.98	2.21e-4	2.96
3	10	1.18e-1	–	7.71e-1	–
	20	1.21e-2	3.29	9.71e-2	2.99
	40	1.17e-3	3.37	1.03e-2	3.23
	80	8.73e-5	3.74	9.08e-4	3.51
	160	5.77e-6	3.92	6.75e-5	3.75
	320	3.65e-7	3.98	4.28e-6	3.98

5.3 Test case 3

This test case was designed to test the robustness and accuracy of the method for non-linear problems with small coefficient for the third derivative term [34, 35]. We compute the soliton solution of the generic KdV equation:

$$u_t+u_x+\left(\frac{u^4}{4}\right)_x+\varepsilon u_{xxx}=0, \tag{5.5}$$

with an initial condition

$$u(x,0)=A\text{sech}^{\frac{2}{3}}(K(x-x_0)),$$

with $A=0.2275$, $x_0=0.5$, $\varepsilon=2.058e-5$ and $K=3\left(A^3/40\varepsilon\right)^{1/2}$. The analytical solution is

$$u(x,t)=A\text{sech}^{\frac{2}{3}}\left(K(x-x_0)-\omega t\right), \tag{5.6}$$

where $\omega=K(1+A^3/10)$.

The following boundary conditions were applied over the interval $[-2,3]$:

$$u(-2,t)=g_1(t), \qquad u_x(3,t)=g_2(t), \qquad u_{xx}(3,t)=g_3(t), \tag{5.7}$$

Table 11: $u_t+u_x+(u^4/4)_x+\varepsilon u_{xxx}=0$, $u(x,0)=A\text{sech}^{2/3}(K(x-x_0))$, with $A=0.2275$, $x_0=0.5$, $\varepsilon=2.058e-5$ and $K=3\left(A^3/40\varepsilon\right)^{1/2}$. Domain over the interval $[-2,3]$. Boundary conditions given in Eq. (5.7). L_2 and L_∞ errors using uniform meshes at $t=1$.

k	Grid	L_2-error	L_2-order	L_∞-error	L_∞-order
1	10	4.25e-2	–	3.83e-1	–
	20	1.60e-2	1.41	1.56e-1	1.29
	40	5.39e-3	1.57	6.06e-2	1.37
	80	1.60e-3	1.75	2.15e-2	1.49
	160	4.45e-4	1.85	7.07e-3	1.61
	320	1.13e-4	1.98	2.00e-3	1.82
	640	2.82e-5	2.00	5.11e-4	1.97
2	10	1.99e-2	–	1.67e-1	–
	20	3.68e-3	2.44	3.37e-2	2.31
	40	7.42e-4	2.31	7.35e-3	2.20
	80	1.39e-4	2.41	1.42e-3	2.37
	160	2.05e-5	2.77	2.49e-4	2.51
	320	2.63e-6	2.96	3.56e-5	2.81
	640	3.31e-7	2.99	4.51e-6	2.98
3	10	1.66e-2	–	1.46e-1	–
	20	1.93e-3	3.11	2.17e-2	2.77
	40	1.69e-4	3.51	2.69e-3	3.01
	80	1.22e-5	3.79	2.60e-4	3.37
	160	7.90e-7	3.95	1.91e-5	3.77
	320	4.98e-8	3.99	1.27e-6	3.91
	640	3.11e-9	4.00	7.98e-8	3.99

Table 12: $u_t+u_x+(u^4/4)_x+\varepsilon u_{xxx}=0$, $u(x,0)=A\text{sech}^{2/3}(K(x-x_0))$, with $A=0.2275$, $x_0=0.5$, $\varepsilon=2.058e-5$ and $K=3\left(A^3/40\varepsilon\right)^{1/2}$. Domain over the interval $[-2,3]$. Boundary conditions given in Eq. (5.7). L_2 and L_∞ errors using non-uniform (repeating pattern of $0.9\Delta x$ and $1.1\Delta x$) meshes at $t=1$.

k	Grid	L_2-error	L_2-order	L_∞-error	L_∞-order
1	10	4.45e-2	–	4.15e-1	–
	20	1.74e-2	1.35	1.74e-1	1.25
	40	6.17e-3	1.50	6.99e-2	1.32
	80	1.90e-3	1.70	2.56e-2	1.45
	160	5.38e-4	1.82	8.56e-3	1.58
	320	1.38e-4	1.96	2.44e-3	1.81
	640	3.46e-5	2.00	6.23e-4	1.97
2	10	2.53e-2	–	2.09e-1	–
	20	4.61e-3	2.46	4.32e-2	2.28
	40	9.17e-4	2.33	9.27e-3	2.22
	80	1.77e-4	2.37	1.84e-3	2.33
	160	2.69e-5	2.72	3.32e-4	2.47
	320	3.51e-6	2.94	4.77e-5	2.80
	640	4.45e-7	2.98	6.10e-6	2.97
3	10	2.09e-2	–	1.85e-1	–
	20	2.57e-3	3.03	2.85e-2	2.70
	40	2.37e-4	3.44	3.64e-3	2.97
	80	1.76e-5	3.75	3.70e-4	3.30
	160	1.18e-6	3.90	2.83e-5	3.71
	320	7.47e-8	3.98	1.92e-6	3.88
	640	4.67e-9	4.00	1.21e-7	3.99

where $g_i(t)$ is obtained from the analytical solution.

The L_2 and L_∞ errors and orders of accuracies of the numerical solution at $t=1$ second are given in Tables 11-13. Once again, it can be seen that a full $(k+1)^{\text{th}}$ order of accuracy is asymptotically attained for the formulation with k^{th} degree polynomial for both the uniform and the non-uniform meshes.

6 Conclusions

In the present study, we implemented a LDG based formulation for solving equations containing higher spatial derivative terms in a spectral volume context. A linear Fourier analysis was performed to study the dispersion and the dissipation properties of this new formulation. The Fourier analysis was used to eliminate all the unstable SV partitions. The partition resulting in the lowest (spatial) error was selected as the optimal partition. This is reasonable since the spatial errors are universal, i.e., present in all types of time integration methods. The maximum non-dimensional time step for obtaining stable solutions was computed. It was observed that the formulation is stable for a small range of non-dimensional time steps, which are higher than the computed stability cut-offs.

Numerical experiments were conducted to illustrate the accuracy, capability and robustness of this new formulation. Expected orders of accuracy were attained asymptot-

Table 13: $u_t+u_x+(u^4/4)_x+\varepsilon u_{xxx}=0$, $u(x,0)=A\text{sech}^{2/3}(K(x-x_0))$, with $A=0.2275$, $x_0=0.5$, $\varepsilon=2.058e-5$ and $K=3\left(A^3/40\varepsilon\right)^{1/2}$. Domain over the interval $[-2,3]$. Boundary conditions given in Eq. (5.7). L_2 and L_∞ errors using non-uniform (repeating pattern of $0.7\Delta x$ and $1.3\Delta x$) meshes at $t=1$.

k	Grid	L_2-error	L_2-order	L_∞-error	L_∞-order
1	10	4.86e-2	–	5.14e-1	–
	20	2.08e-2	1.22	2.22e-1	1.21
	40	7.97e-3	1.39	9.28e-2	1.26
	80	2.58e-3	1.63	3.52e-2	1.40
	160	7.55e-4	1.77	1.19e-2	1.56
	320	1.98e-4	1.93	3.45e-3	1.79
	640	4.99e-5	1.99	8.87e-4	1.96
2	10	3.47e-2	–	3.16e-1	–
	20	6.49e-3	2.42	6.42e-2	2.30
	40	1.30e-3	2.32	1.31e-2	2.29
	80	2.63e-4	2.30	2.76e-3	2.25
	160	4.26e-5	2.63	5.16e-4	2.42
	320	5.75e-6	2.89	7.56e-5	2.77
	640	7.49e-7	2.94	1.02e-5	2.89
3	10	3.18e-2	–	2.94e-1	–
	20	4.12e-3	2.95	4.85e-2	2.60
	40	4.09e-4	3.33	6.50e-3	2.90
	80	3.26e-5	3.65	6.93e-4	3.23
	160	2.26e-6	3.85	5.52e-5	3.65
	320	1.45e-7	3.96	3.80e-6	3.86
	640	9.08e-9	4.00	2.41e-7	3.98

ically for both the linear and the non-linear equations. In addition, the formulation was able to handle stiff convection dominated cases where the coefficients of the third spatial derivative terms are small.

Future work will include implicit time discretization procedures, employing other flux formulations (like extensions of the BR2 and the penalty scheme), performing Fourier analysis for 2D problems, implementing a p-multigrid algorithm and extending the formulation to equations containing fourth order spatial derivative terms.

The final goal of this research project is to extend this formulation to handle interactions of non linear KDV type waves with multiphase flows [4], explosions [2, 3] and turbulence models [2, 3].

Appendix

A.1 Matrices used in second order Fourier analysis

$$A=\begin{bmatrix}0&0\\0&0\end{bmatrix},\ B=\begin{bmatrix}7&3\\0&0\end{bmatrix},\ C=\begin{bmatrix}-35&+33\\-2&-10\end{bmatrix},\ D=\begin{bmatrix}-7&-3\\28&-20\end{bmatrix},\ E=\begin{bmatrix}3&-1\\6&-2\end{bmatrix}.$$

A.2 Matrices used in third order Fourier analysis ($d=0.1$)

$$A=\begin{bmatrix} 0 & 0 & 0 \\ 0 & 0 & 0 \\ 0 & 0 & 0 \end{bmatrix},$$

$$B=\begin{bmatrix} 7.948325184135814 & 36.16450093538303 & 89.03973788368817 \\ 0 & 0 & 0 \\ 0 & 0 & 0 \end{bmatrix},$$

$$C=\begin{bmatrix} -1204.618702161519 & 1677.274816455901 & -670.0657197540336 \\ 84.22765672321280 & -148.4655284315556 & 71.58994528981473 \\ -16.57893576324851 & 24.26287605275688 & -51.49970467670405 \end{bmatrix},$$

$$D=\begin{bmatrix} 35.76764295428119 & 43.74239590395953 & -18.39336011333079 \\ 37.71608531683748 & -67.14571815374435 & 24.65144840006793 \\ 171.9427405397058 & -189.4845831645637 & 67.03209291593313 \end{bmatrix},$$

$$E=\begin{bmatrix} 4.645457091371171 & -2.168731107174263 & 0.6636367273387380 \\ -3.807487439402157 & 1.777525071826559 & -0.5439267770574504 \\ -8.394119789166726 & 3.918793855168213 & -1.199159969880959 \end{bmatrix}.$$

A.3 Matrices used in fourth order Fourier analysis ($d=0.1$)

$$A=\begin{bmatrix} 0 & 0 & 0 & 0 \\ 0 & 0 & 0 & 0 \\ 0 & 0 & 0 & 0 \\ 0 & 0 & 0 & 0 \end{bmatrix},$$

$$B=\begin{bmatrix} 63.79012345681466 & -221.6056241427161 & 698.5054869684837 & 521.6556927297700 \\ 0 & 0 & 0 & 0 \\ 0 & 0 & 0 & 0 \\ 0 & 0 & 0 & 0 \end{bmatrix},$$

$$C=\begin{bmatrix} -3121.465569273001 & 3290.440877914971 & -1973.603566529508 & 871.9368998628328 \\ 64.86913580247066 & -153.0063100137205 & 179.61591220850572 & -43.67626886145311 \\ 11.23950617283643 & 0.7879286694173029 & -101.2565157750393 & -25.93141289437598 \\ -70.72345679014046 & 233.3784636488701 & -504.3326474622926 & -439.7791495198968 \end{bmatrix},$$

$$D=\begin{bmatrix} -116.1912208504799 & -24.79574759945215 & 19.93758573388266 & -15.71604938271646 \\ -125.8743484224965 & 119.3421124828523 & -64.92455418381312 & 29.87654320987638 \\ 354.4548696845022 & -366.7484224965725 & 200.9849108367643 & -93.97530864197615 \\ 1826.710013717431 & -1593.468587105628 & 860.2647462277143 & -389.1604938271629 \end{bmatrix},$$

$$E=\begin{bmatrix} 10.03456790123468 & -4.306172839506221 & 2.093827160493855 & -0.7111111111111191 \\ -8.780246913580134 & 3.767901234567852 & -1.832098765432079 & 0.6222222222222142 \\ 28.84938271604949 & -12.38024691358029 & 6.019753086419790 & -2.044444444444452 \\ 108.8123456790123 & -46.69506172839506 & 22.70493827160501 & -7.711111111111111 \end{bmatrix}.$$

References

[1] R. Abgrall, On essentially non-oscillatory schemes on unstructured meshes: analysis and implementation, J. Comput. Phys., 114 (1994), 45–58.

[2] K. Balakrishnan and S. Menon, On the role of ambient reactive particles in the mixing and afterburn behind explosive blast waves, Combust. Sci. Technol., 182 (2010), 186–214.
[3] K. Balakrishnan, F. Genin, D. V. Nance and S. Menon, Numerical study of blast characteristics from detonation of homogeneous explosives, Shock Waves, 20(2) (2010), 147–162.
[4] K. Balakrishnan and S. Menon, On turbulent chemical explosions into dilute aluminum particle clouds, Combust. Theor. Model., 14(4) (2010), 583–617.
[5] T. J. Barth and P. O. Frederickson, High-order solution of the Euler equations on unstructured grids using quadratic reconstruction, AIAA 90-0013, 1990.
[6] B. Cockburn and C. W. Shu, Runge-Kutta discontinuous Galerkin methods for convection-dominated problems, J. Sci. Comput., 16(3) (2001), 173–261.
[7] B. Cockburn and C.-W. Shu, The local discontinuous Galerkin method for time-dependent convection diffusion system, SIAM J. Numer. Anal., 35 (1998), 2440–2463.
[8] M. Delanaye and Y. Liu, Quadratic reconstruction finite volume schemes on 3D arbitrary unstructured polyhedral grids, AIAA 99-3259-CP, 1999.
[9] R. Harris, Z. J. Wang and Y. Liu, Efficient quadrature-free high-order spectral volume method on unstructured grids: theory and 2D implementation, J. Comput. Phys., 227 (2008), 1620–1642.
[10] R. Harris and Z. J. Wang, High-order adaptive quadrature-free spectral volume method on unstructured grids, Comput. Fluids, 38 (2009), 2006–2025.
[11] A. Harten, B. Engquist, S. Osher and S. Chakravarthy, Uniformly high order essentially non-oscillatory schemes III, J. Comput. Phys., 71 (1987), 231–303.
[12] R. Kannan, An implicit LU-SGS spectral volume method for the moment models in device simulations: formulation in 1D and application to a p-multigrid algorithm, Int. J. Numer. Methods Biomedical Eng., accepted on 11 Oct. 2009, published online: 1 Feb. 2010.
[13] R. Kannan, An implicit LU-SGS s Volume method for the moment models in device simulations II: accuracy studies and performance enhancements using the penalty and the BR2 formulations, Int. J. Numer. Methods Biomedical Eng., accepted August 2010.
[14] R. Kannan and Z. J. Wang, A study of viscous flux formulations for a p-multigrid spectral volume Navier stokes solver, J. Sci. Comput., 41(2) (2009), 165–199.
[15] R. Kannan and Z. J. Wang, LDG2: a variant of the LDG flux formulation for the spectral volume method, J. Sci. Comput., published online 20th June 2010.
[16] R. Kannan and Z. J. Wang, The direct discontinuous Galerkin (DDG) viscous flux scheme for the high order spectral volume method, Comput. Fluids, article in press (doi:10.1016/j.compfluid.2010.07.006).
[17] R. Kannan, High Order Spectral Volume and Spectral Difference Methods on Unstructured Grids, Ph.D Thesis, Iowa State University, 2008.
[18] C. Liang, R. Kannan and Z. J. Wang, A-p-multigrid spectral difference method with explicit and implicit smoothers on unstructured grids, Comput. Fluids, 38(2) (2009), 254–265.
[19] M.-S.Liou and C. Steffen, A new flux splitting scheme, J. Comput. Phys., 107 (1993), 23–39.
[20] Y. Liu, M. Vinokur and Z. J. Wang, Spectral (finite) volume method for conservation laws on unstructured grids V: extension to three-dimensional systems, J. Comput. Phys., 212 (2006), 454–472.
[21] P. L. Roe, Approximate Riemann solvers, parameter vectors and difference schemes, J. Comput. Phys., 43 (1981), 357–372.
[22] V. V. Rusanov, Calculation of interaction of non-steady shock waves with obstacles, J. Comput. Math. Phys. USSR 1 (1961), 267–279.
[23] C. W. Shu, Total-variation-diminishing time discretizations, SIAM J. Sci. Stat. Comput., 9

(1988), 1073–1084.
[24] Y. Sun and Z. J. Wang, Efficient implicit non-linear LU-SGS approach for compressible flow computation using high-order spectral difference method, Commun. Comput. Phys., 5 (2009), 760–778.
[25] Y. Sun, Z. J. Wang and Y. Liu, Spectral (finite) volume method for conservation laws on unstructured grids VI: extension to viscous flow, J. Comput. Phys., 215 (2006), 41–58.
[26] K. Van den Abeele, T. Broeckhoven and C. Lacor, Dispersion and dissipation properties of the 1D spectral volume method and application to a p-multigrid algorithm, J. Comput. Phys., 224(2) (2007), 616–636.
[27] B. Van Leer, Towards the ultimate conservative difference scheme II: monotonicity and conservation combined in a second order scheme, J. Comput. Phys., 14 (1974), 361–376.
[28] B. Van Leer, Towards the ultimate conservative difference scheme V: a second order sequel to Godunov's method, J. Comput. Phys., 32 (1979), 101–136.
[29] Z. J. Wang, Spectral (finite) volume method for conservation laws on unstructured grids: basic formulation, J. Comput. Phys., 178 (2002), 210–251.
[30] Z. J. Wang and Y. Liu, Spectral (finite) volume method for conservation laws on unstructured grids II: extension to two-dimensional scalar equation, J. Comput. Phys., 179 (2002), 665–697.
[31] Z. J. Wang and Y. Liu, Spectral (finite) volume method for conservation laws on unstructured grids III: extension to one-dimensional systems, J. Sci. Comput., 20 (2004), 137–157.
[32] Z. J. Wang and Y. Liu, Spectral (finite) volume method for conservation laws on unstructured grids IV: extension to two-dimensional Euler equations, J. Comput. Phys., 194 (2004), 716–741.
[33] Z. J. Wang and Y. Liu, Extension of the spectral volume method to high-order boundary representation, J. Comput. Phys., 211 (2006), 154–178.
[34] J. Yan and C. W. Shu, A local discontinuous Galerkin method for KdV type equations, SIAM J. Numer. Anal., 40(2) (2002), 769–791.
[35] J. Yan and H. Liu, A local discontinuous Galerkin method for the Korteweg-de Vries equation with boundary effect, J. Comput. Phys., 215 (2006), 197–218.
[36] M. Zhang and C. W. Shu, An analysis of three different formulations of the discontinuous Galerkin method for diffusion equations, Math. Model. Methods Appl. Sci., 13 (2003), 395–413.